Chapter 4

The Shadow of the Moon

4.1 Introduction

One astronomical object surely visible to an underground muon detector is the Moon. Rather than existing as a traditional astronomical source, however, the Moon is a sink of cosmic rays. As first discussed by Clark in 1957[1], incoming primary cosmic rays are blocked by the Moon, casting a shadow in the cosmic ray sky as seen from Earth. The high energy muons seen by MACRO come primarily from hadronic parents (see Chapter 1). While ambient magnetic fields cause such charged particles to scatter and lose their directionality, the distance between the Earth and Moon is short enough that the parents not blocked by the Moon are not subsequently scattered into the shadow. This allows the shadow to remain well-defined at Earth. All other astronomical objects which might create a feature in the cosmic ray sky are too far away for the charged hadronic parents of the muons observed by MACRO to retain enough of their directionality in the ambient magnetic fields to be detected with MACRO’s currently available statistics. This includes the Sun, as discussed in Section 4.5.

Observing the Moon in the muon sky provides a good check on an experiment's ability to locate astronomical point sources of muons. If a detector can find the Moon's shadow in its data, then the whole process of turning particle hits inside that detector into muon tracks that point back onto the sky has been validated. Most important, an observation of the Moon confirms the detector's pointing, and helps to establish its sensitivity. This calibration allows a search for more interesting astronomical sources to be performed with the confidence that should there be such sources at detectable signal strengths, the experiment and data analysis path will find them.

What makes this problem more difficult for MACRO than for the surface air shower arrays that saw this effect in the past[2,3,4,5] is lower statistics. Underground detectors necessarily have a smaller effective area than surface arrays, thus collecting far fewer events. Additionally, air shower arrays have a higher energy threshold (observing muons from primaries of ≥100 Tev rather than ≥2 TeV). Higher energy cosmic rays travel more direct paths to the detector, providing a cleaner signal.

Observing the Moon's shadow with MACRO is not as straightforward as it might first seem. The Moon's disk subtends ~0.5° on the sky. Although any given muon passing through MACRO can be reconstructed and its path projected back onto the sky with a geometrically limited resolution of 0.2°[6] (as shown in Chapter 6), that muon has arrived at the detector after passing through an average of 3800 mwe of rock overburden. As the muon traverses the rock, it is subjected to multiple Coulomb scattering[7]. This reduces MACRO's effective angular resolution to ~1° (see chapter 6), which is larger than the Moon's apparent size. Before traversing the rock, the Moon's shadow in the high energy muon sky would be a comparatively sharp disk. However, passage of the muons through the rock causes many muons to be scattered into the shadow. This results in an overall deficit of muons from the direction of the Moon, but not a cleanly defined shadow.

4.2 The Data

4.2.1 Collecting the Muons

Using the data analysis path described in chapter 3, MACRO collected 31.4 million muons from February 1989 through December 1994. This process generated a list of good muon events tagged with the time, zenith and azimuthal angles of the event. For this analysis, the position of the Moon at the time of the arrival of each muon was calculated using the database of ephemerides available from the Jet Propulsion Laboratory, JPLEPH[8].

As described by Duffett-Smith[9], corrections for the parallax caused by MACRO's location on the Earth were applied to the ephemeris position. The position of the Moon is calculated by the ephemeris with respect to the center of the Earth. However, the vector from Earth's center to MACRO will cause the actual position of the Moon on the sky as seen from MACRO to be different than that calculated by the center-to-center ephemeris by up to 1°. To correct for this parallax, MACRO's altitude above sea level of 930 m was added to the radius of the Earth as corrected for the Earth's non-spherical figure at MACRO's latitude. This gives the magnitude of the Earth-MACRO vector; its direction is calculable from the local sidereal time. The Earth-Moon vector (including the varying distance to the Moon due to its elliptical orbit) is returned by the ephemeris. Thus, the parallax correction needed is the angle the Earth-Macro vector subtends from the Earth-Moon vector. As a side benefit, the exact angular size subtended by the Moon's disk can be calculated, because the exact MACRO-Moon distance is now known. This is useful later in this analysis, during the simulation of the Moon's shadow.

Once the ephemeris position of the Moon was corrected for parallax, the difference in space angle between the muon and the Moon was stored in a two dimensional histogram of dimensions 10.1° on a side, binned at 0.2° per bin. The angles calculated were:

$$\begin{aligned} \Delta\alpha &= (\alpha_{\mu} - \alpha_{moon}) \sin(\delta_{moon}) \\ \Delta\delta &= (\delta_{\mu} - \delta_{moon}) \end{aligned} \qquad \textbf{(1)}$$

where α is right ascension and δ is declination. The 0.2° binning was chosen to match the geometrical tracking resolution of MACRO (Chapter 6). In addition to putting the muons near the Moon into this histogram, twenty other histograms were made. The first ten were identical windows on the sky, but displaced in α. The second ten came from the declination band just above that occupied by the Moon and the first ten windows. These twenty other histograms were made as control frames, that is, to provide data samples containing no source. In addition, this whole binning process was repeated in a different coordinate system, using altitude (θ) in place of δ, and azimuth (ϕ) in place of α. This coordinate transformation should not affect the results of the analysis, but comparing the results in the two coordinate systems could uncover systematics introduced by the data binning.

4.2.2 **Determining The Backgrounds**

To understand what the sky would look like if the Moon's shadow was not present, the Monte Carlo method described in Chapter 3 was used to generate complete data sets of 31.4 million simulated muons. These muons were analyzed the same way as the real data, and binned into the same histograms. There were 560 such simulated data sets generated, with the resulting histograms averaged to suppress statistical fluctuations by a factor of $\sqrt{560}$. This resulted in histograms containing the number of muons per bin that would be expected in the absence of any real signals or statistical fluctuations.

4.2.3 **The Expected Shadow of the Moon**

To understand what happens to the paths of muons as they scatter through the mountain, double muons from the real data were investigated in more detail. Double muons are pairs created together in the cascade initiated by the interaction of a primary cosmic ray nuclei with the upper atmosphere. At the time these muons are created, they travel in nearly parallel paths[10]. When they arrive at MACRO, their paths are no longer parallel due to multiple coulomb scattering. Thus the distribution of angles observed between double muons when they arrive at MACRO is a good representation of the scattering any individual muon suffers from the mountain, after the distribution is divided by a factor of $\sqrt{2}$ to account for the scattering happening to both muons in a real pair. An example of this distribution is shown in Figure 1. This is assumed to be MACRO's point spread function (PSF).

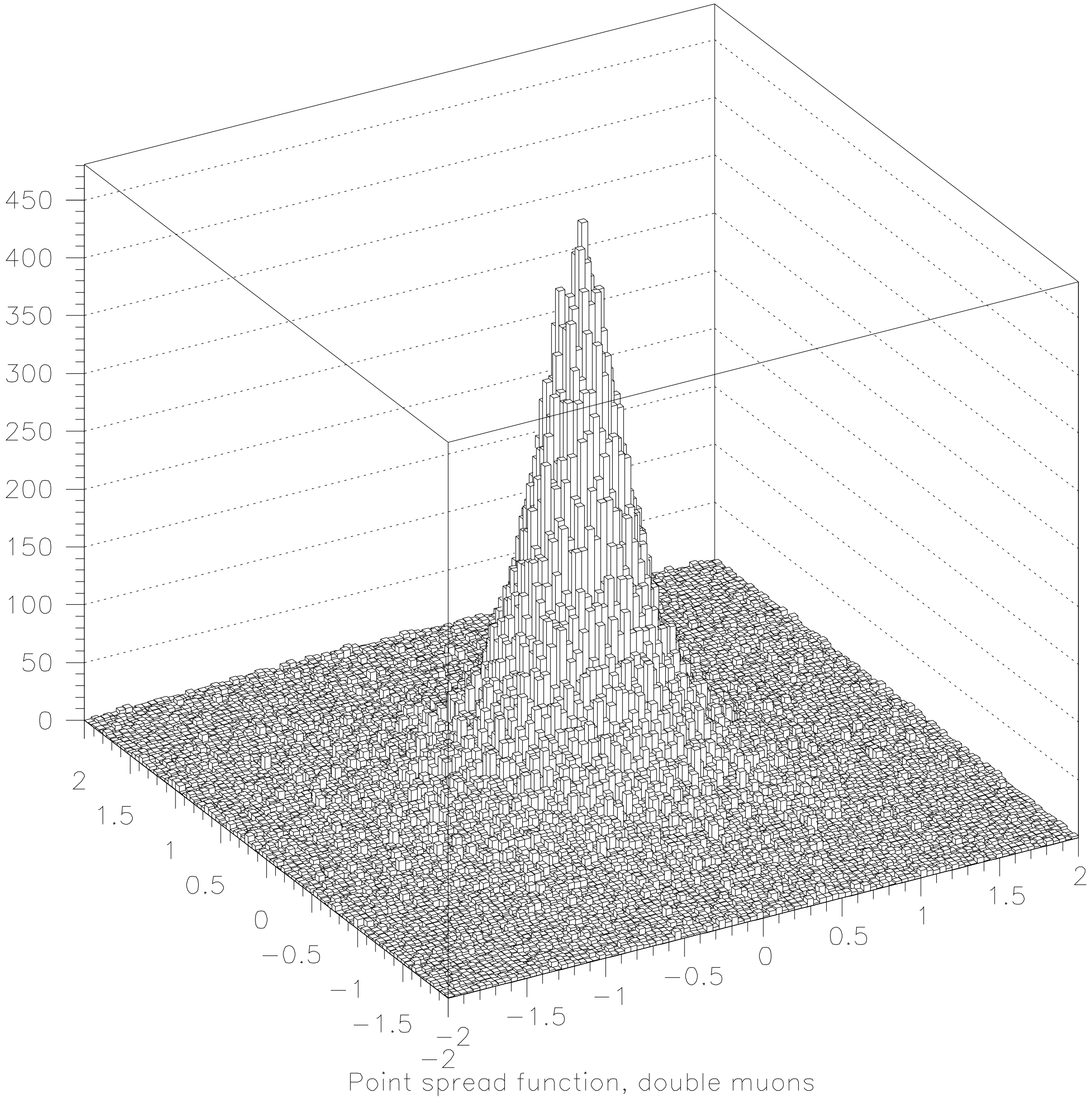

Figure 1: The 2D distribution of space angles in degrees between double muons from the complete MACRO, divided by √2. This is assumed to be MACRO's point spread function (PSF).

The addition of the attico (see Chapter 2) to the lower half of the detector changed MACRO's PSF. While the central degree of the distribution became sharper,

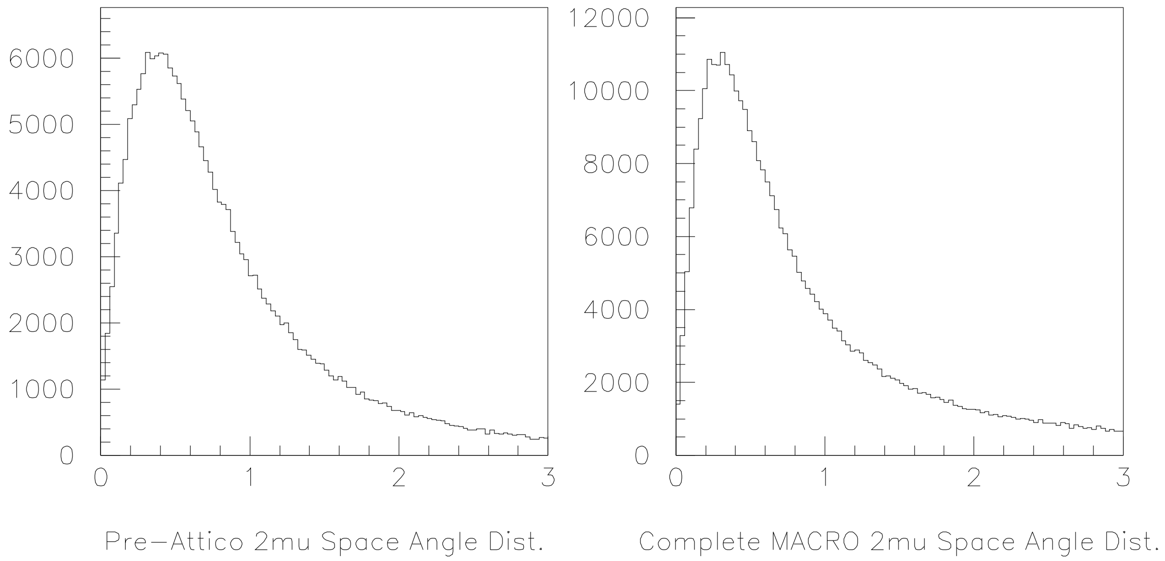

Figure 2: One dimensional projections of the double muon space angle distributions in degrees for pre-attico and complete MACRO data samples.

the tails of the distribution became longer. This is shown in one dimensional projections in Figures 2a and 2b. The central part of this distribution tightened as expected. The addition of the attico allowed a longer lever arm to fit tracks that passed through both the attico and lower detectors more accurately. The longer tails were unexpected, and were therefore examined closely. After hand-scanning many events with large double muon angular separations, it was found that the vast majority of such events were of a class where at least one of the muons involved fell onto MACRO passing either solely through the attico or along a vertical face. A muon track which passes only through the attico has fewer hit points and a short lever arm. These factors make for a much less reliable fit, increasing the error in resolving the angular separation of the two muons and widening the tails of the distributions. To take this difference in PSFs into account in this analysis, two different PSFs were made for each detector configuration. Data collected with the lower half of MACRO used a PSF derived from double muons observed with that detector configuration. Data taken after the introduction of the attico used a PSF constructed from that data set.

This PSF was used in Monte Carlo studies to simulate what the shadow of the Moon might look like. After each simulated muon was binned in space relative to the position of the Moon, the shadow of the Moon was introduced. If the simulated muon's direction was coming from a point on the sky that would have been eclipsed by the Moon's disk, it was eliminated from the sample. All remaining simulated muons were scattered in α and δ by a displacement chosen from a PSF, as shown in Figure 1. The exact PSF used for this scatter was the appropriate one for MACRO's detector configuration for the time period being simulated. These newly scattered muons were binned into another histogram of position versus that of the Moon. This simulates the process by which real muons are scattered into the Moon's shadow by the rock overburden. This histogram of the expected Moon shadow was created for each of the 560 separate simulations; to reduce statistical fluctuations these were then

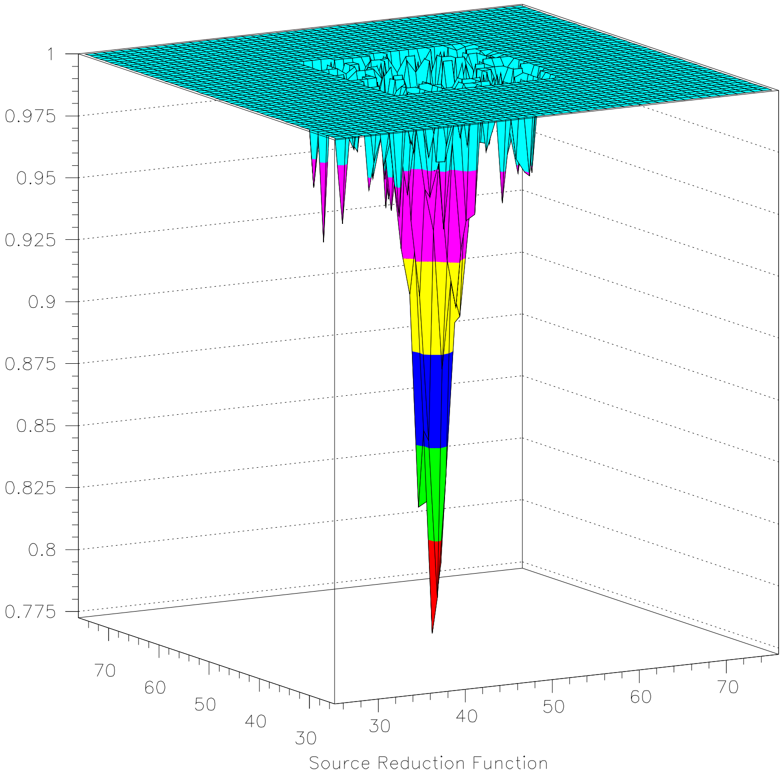

Figure 3: I_s, the source reduction function, which is the expected moon shadow.

averaged. The resulting expected shadow of the Moon is shown in Figure 3. This is the expected shadow if MACRO had 560 times more data, or nearly 2000 years of additional live time. The practical use of this information is to generate the expected shape of the Moon's shadow, for use in the log-likelihood fit in Section 4.3.

4.3 The Maximum Likelihood Analysis

A maximum likelihood test was used to search the data for the Moon. The data, backgrounds, and simulated Moon shadow were the inputs to this test. This test is described in detail by Cash[11] and was used by the COS-B gamma ray satellite observers to search their data for sources[12]. The test examines each bin of a data minus background image for how well it and the surrounding bins fit the hypothesis that a signal of some known shape is centered at that bin. The value calculated is the log-likelihood function for the Poissonian process,

$$\lambda(x_s,y_s,I_s) = 2\sum_{i=1}^{n_i}\left[N_i^{th} - N_i^{obs} + N_i^{obs}\ln\left(\frac{N_i^{obs}}{N_i^{th}}\right)\right] . \qquad \textbf{(2)}$$

The number of expected counts in the presence of a signal sink, N_i^{th}, is given by

$$N_i^{th} = N_i^{back}\left[1 - I_s(x_i - x_s, y_i - y_s)\right] , \qquad \textbf{(3)}$$

where (x_s,y_s) is the test position of the source; (x_i,y_i) is the position of bin i; N_i^{obs} is the number of counts observed in that bin; N_i^{back} is the expected background in the absence of a source; I_s is the source reduction factor; and the sum is over n_i, all bins used to compute I_s. The source reduction term is taken from the expected moon shadow as computed by Monte Carlo simulation. It is represented by a fractional deficit for each bin as a function of position relative to the center bin of the simulated Moon shadow, shown in Figure 3.

Qualitatively, the λ function represents how well the expected source signal I_s fits to a position x_s,y_s in the image. In addition, $\lambda(x_s,y_s,0)$ is computed. This quantity is $\lambda(x_s,y_s,I_s)$ evaluated with no reduction. This term quantifies how well the data fits the hypothesis of no source at all centered on the point in question. Then, for each bin the value

$$\Lambda = \lambda(x_s,y_s,I_s) - \lambda(x_s,y_s,0) \tag{4}$$

is computed. This subtraction gives the likelihood that a source of shape I_s fits the data in the vicinity of (x_s,y_s) better than does an assumption of no source. The larger the value of Λ, the better the data surrounding this particular bin fits the modeled Moon shadow. If Λ is negative, then the data at that point is best explained by no shadow at all. This analysis was done first on the data binned in α and δ, and again in the θ and ϕ coordinate system. The equatorial coordinates α and δ are the important coordinates for any astronomical search, but the answer should be similar in both coordinate systems. The values of Λ in the five degrees in α and δ surrounding the Moon are shown in Figure 4, and in θ and ϕ in Figure 5.

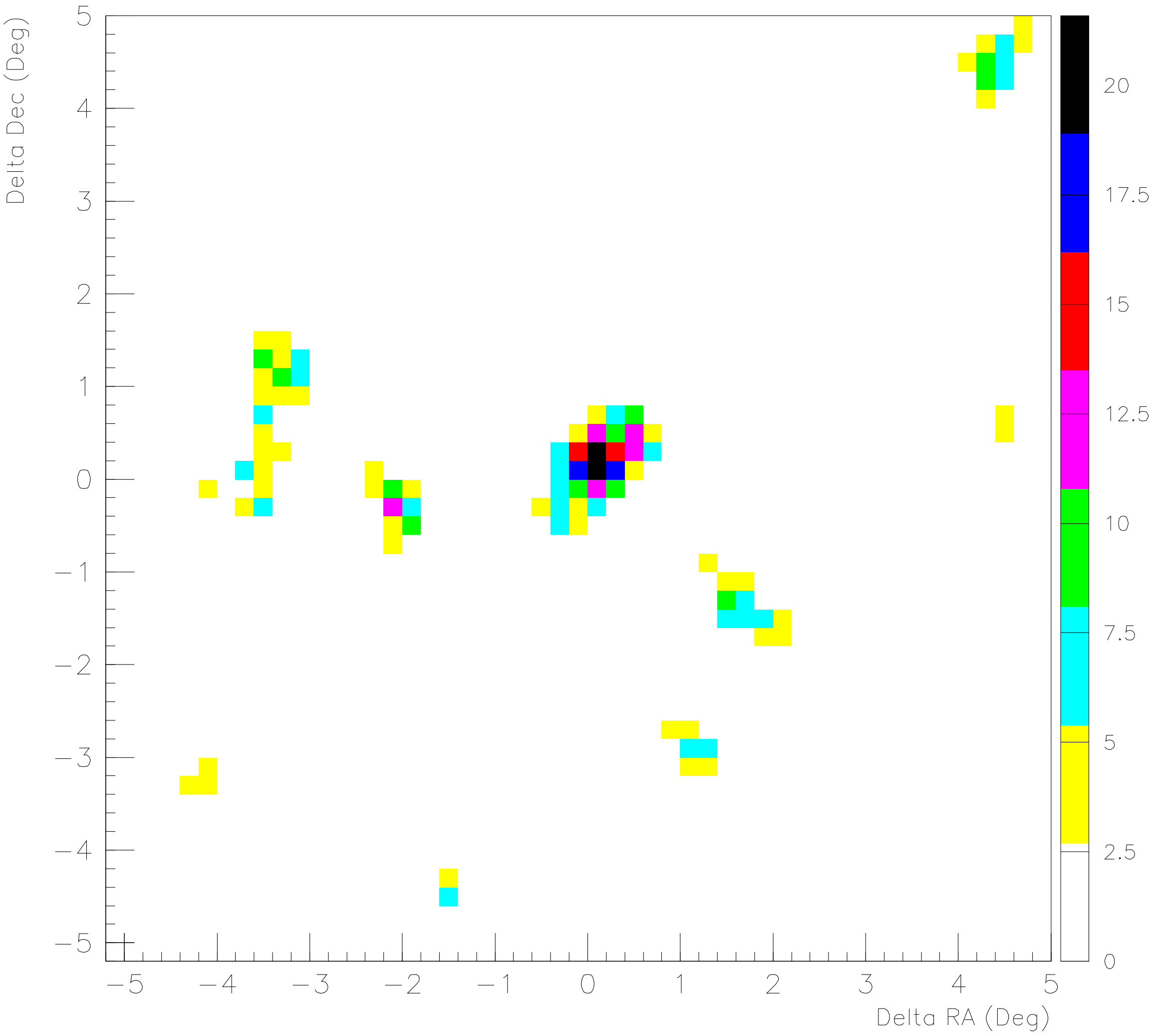

Figure 4: The map of Λ in Δα and Δδ, 0.2° bins.

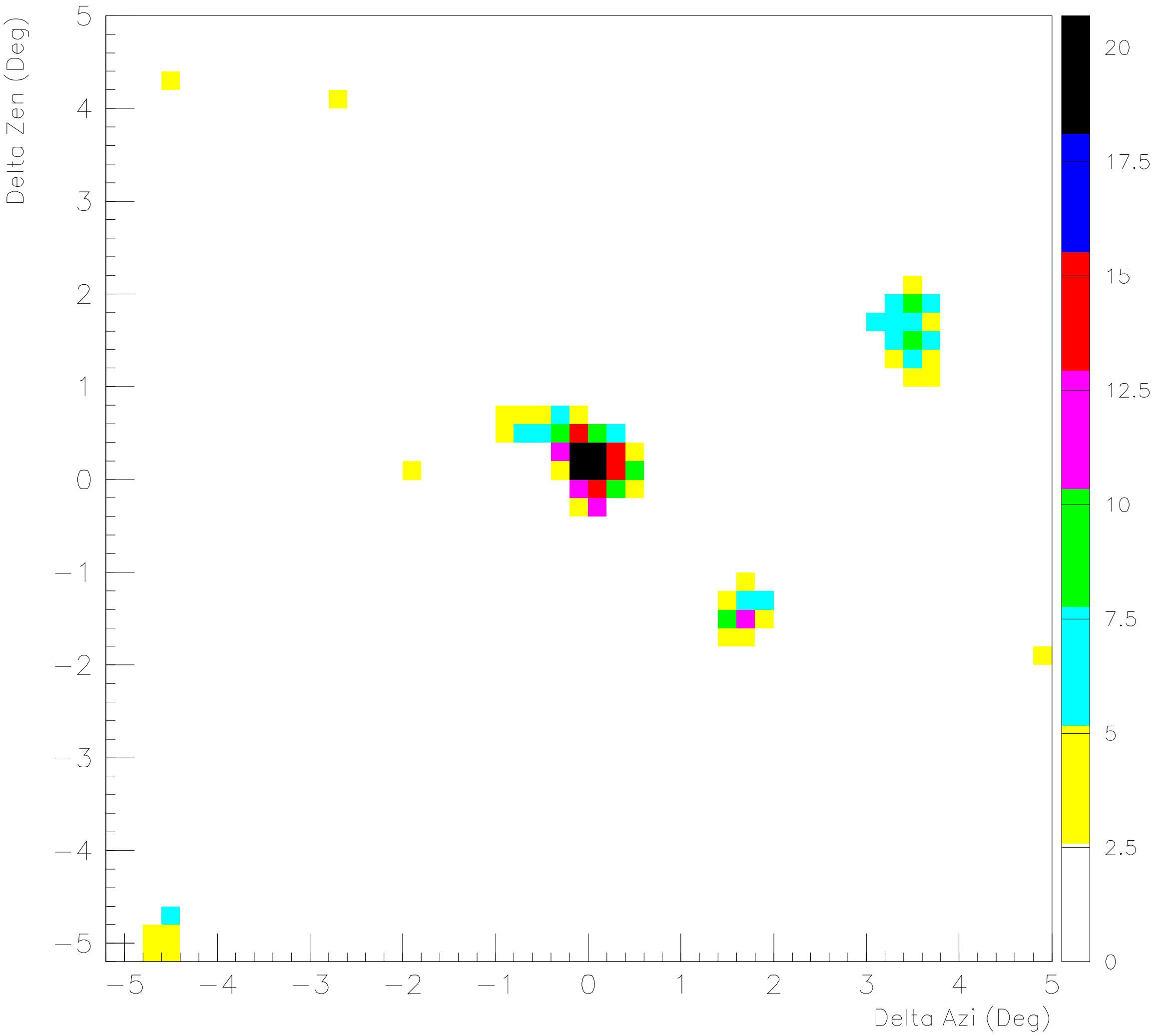

Figure 5: The map of Λ in $\Delta\phi$ and $\Delta\theta$, 0.2° bins.

4.4 Interpreting the Results

The maximum values for Λ found near the Moon are shown in Table 1.

Survey	Λ_{moon}	Δposition	MC Probability (Section 4.4.1)	Combined MC and Geometrical Prob. (Section 4.4.2)
(α,δ)	21.6	(+0.0°,+0.2°)	2.40e-04	5.40e-06
(θ,ϕ)	20.7	(+0.0°,+0.0°)	2.89e-04	6.51e-06

Table 1: Results of Λ Surveys

The locations that best fit the calculated Moon shadow shapes lie within one bin of the Moon's true location. Since the size of one bin is the geometrical angular resolution of MACRO's tracking system and the Moon's location is centered in the middle bin, the best fit location for the Moon at one bin (0.2°) to one side is considered on target within MACRO’s geometrical resolution. The Moon’s shadow is seen exactly where it should be seen.

4.4.1 Significance as Determined via Monte Carlo

However, ignoring for the moment the fact that the observed moon shadow lies exactly where it should, what is the significance of the Λ numbers? One can see several other regions of nonzero Λ in Figures 4 and 5. There is a chance that such background fluctuations can mimic the signal expected by the Moon. In fact, when repeating the maximum likelihood analysis in the twenty (α,δ) off-source windows, there is one window containing a maximum Λ of a comparable value (19.0) to that in the window directly surrounding the Moon (21.6).

In order to quantify the chance that a background fluctuation could mimic the shadow of the moon, many random background fluctuations were generated by simulating Poissonian fluctuations of the expected backgrounds in each bin of the two surveys. These simulated datasets contain no sources or shadows, only statistical fluctuations that may mimic the Moon shadow. Each data set was binned into the same twenty off-source windows on the sky as the real data. These windows were subdivided into four independent areas of 2° on a side. This is the size of the expected Moon shadow template in use. For the total of 1771 simulated data sets, this resulted in 141,680 maximum likelihood calculations in windows the size of the search immediately around the Moon. Of those 141,680 samples of moonless data, Λ_{max} of a value greater than or equal to that seen at the position of the Moon occurred 34 times in the (α,δ) survey, and 41 times in the (θ,ϕ) survey. The complete distribution of the Λ_{max} values due to fluctuations is shown in Figures 6a and 6b. The entries in Table 1 under the heading "MC Probability" represent the division of the number of

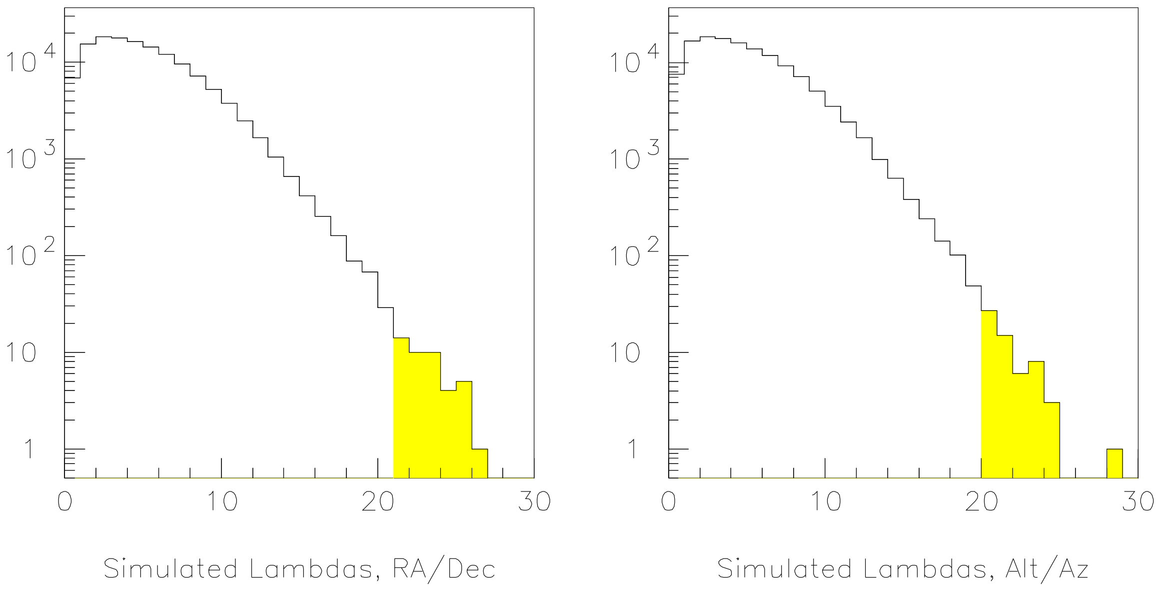

Figure 6: The distribution of Λ_{max} arising from Poissonian fluctuations in expected background counts. Values of Λ_{max} equal to or greater than that observed near the real moon are highlighted.

occurrences of $\Lambda_{max} \geq \Lambda_{moon}$ by the number of trials.

4.4.2 Significance of the Correct Moon Location

The Monte Carlo calculation of the significance of the log-likelihood result does not take into account the fact that this procedure finds the Moon in the expected position on the sky. Given the geometrical track resolution of 0.2°, and the bin-center to bin-center distance of the same amount, any one of the nine center bins in the image would be considered "on target". The position of Λ_{max} in both surveys meets this criterion.

The log-likelihood procedure searched areas the size of the I_s template (2°x2°) during the significance calculation and recorded the statistical fluctuation induced Λ_{max} in each of these windows for later comparison with the Λ_{max} observed at the Moon's position. There are 400 0.2° bins in the I_s template. If the center nine would be considered “on target”, then there is a 9/400 or 2.25×10^{-2} chance that a background fluctuation in this area would fall “on target” by chance. These geometrical odds are multiplied with the chance calculated by Monte Carlo for getting a fluctuation of the listed significance or higher from Section 4.4.1. This results in the probability of a background fluctuation of this magnitude occurring at just the right location in the sky, and is listed in the last column of Table 1. Such a low chance of the real data’s Λ_{max} being mimicked by a statistical fluctuation strongly supports the validity of MACRO’s observation of the Moon’s shadow.

4.4.3 **Significance Determined using √N Statistics**

For another check with a simpler, more easily understood statistical method, the number of muons missing from the vicinity of the Moon has been calculated using familiar √N statistics. The space angle from each bin in the Moon's window to the bin containing Λ_{max} was computed. The number of muons in the real data minus the simulated background for each bin centered at a given radius were averaged together

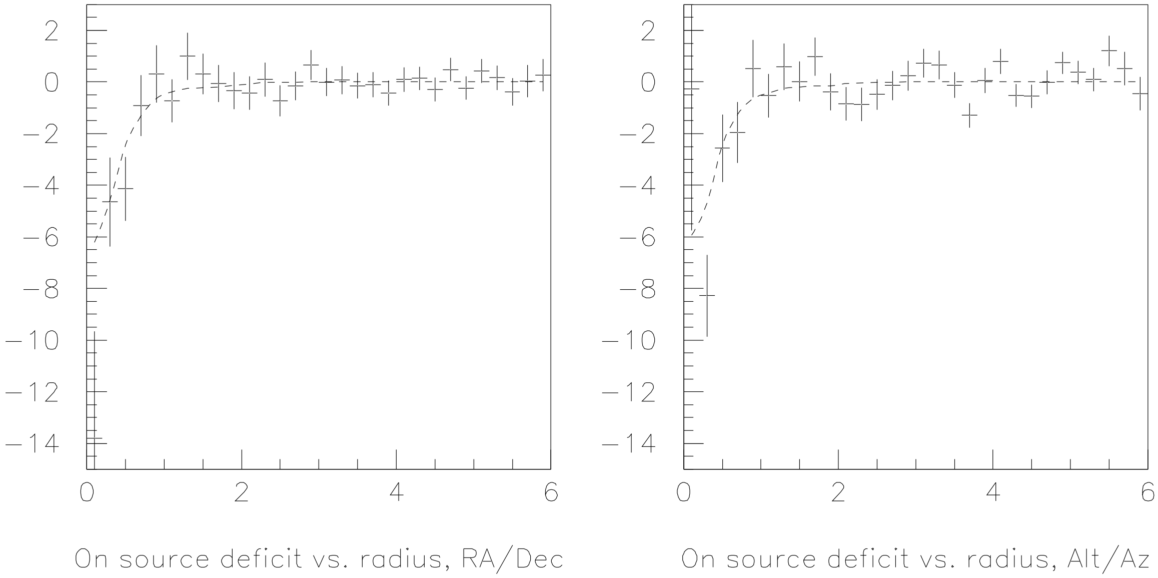

Figure 7: The average deficit of muons per 0.2° bin vs. Radius from the moon in degrees, each survey.

and plotted versus radius in Figure 7.

There is a deficit of muons in the first few bins in radius. As radius increases, more solid angle contributes to the average at that radius. This causes the statistical error $\sqrt{N_{obs}}$ on the average to decrease, as can be seen by the error bars in the figure. The same procedure was repeated using the expected Moon shadow used for the maximum likelihood fit. This expected deficit is superimposed as a smooth line upon the figure.

The total deficit that can be attributed to the Moon is calculated by integrating the deficit as a function of radius from 0° to 0.8°. This is the radius where the wings of the Moon shadow become lost in the noise. This process produces the numbers observed and expected in the absence of the Moon listed in Table 2. These numbers are large enough for Gaussian statistics to be valid, so the deficit can be expressed as a ΔN/√N deviation. The probability that such a deviation can be the result of a Gaussian fluctuation is also given. This significance is comparable to the significance computed by Monte Carlo from the maximum likelihood analysis and listed in Table 1. The agreement between these different methods of computing a significance for the detection of the Moon's shadow is heartening.

	N_{obs}	N_{back}	σ	Prob.
(α,δ)	1343	1484	-3.83	1.26e-04
(θ,ϕ)	1324	1477	-4.22	2.46e-05

Table 2: √N Statistics

4.5 The Shadow of the Sun

Observing the shadow of the Sun is a good deal harder than observing the Moon’s, even though both objects subtend the same ~0.5° disk on the sky. While the air shower experiments referenced in Section 4.1 gathered enough statistics and have sufficient resolution needed to see the Sun’s shadow, their Sun observations remain far less significant than their Moon observations. This problem is due to the Sun’s magnetic field, as discussed by the CASA collaborators[5]. The MACRO observation of the Moon is far less significant than similar air shower observations, and MACRO has been unable to observe the Sun’s shadow. The same maximum likelihood analysis that was done for the Moon has been done for the sun. The one difference between the two procedures was that fewer simulations (120 instead of 560) were averaged to determine the backgrounds. A map of Λ near the Sun’s position on the sky is shown in Figure 8. Λ_{max} in this figure is 13.0. This is statistically insignificant, as can be verified by comparison with Figure 6.

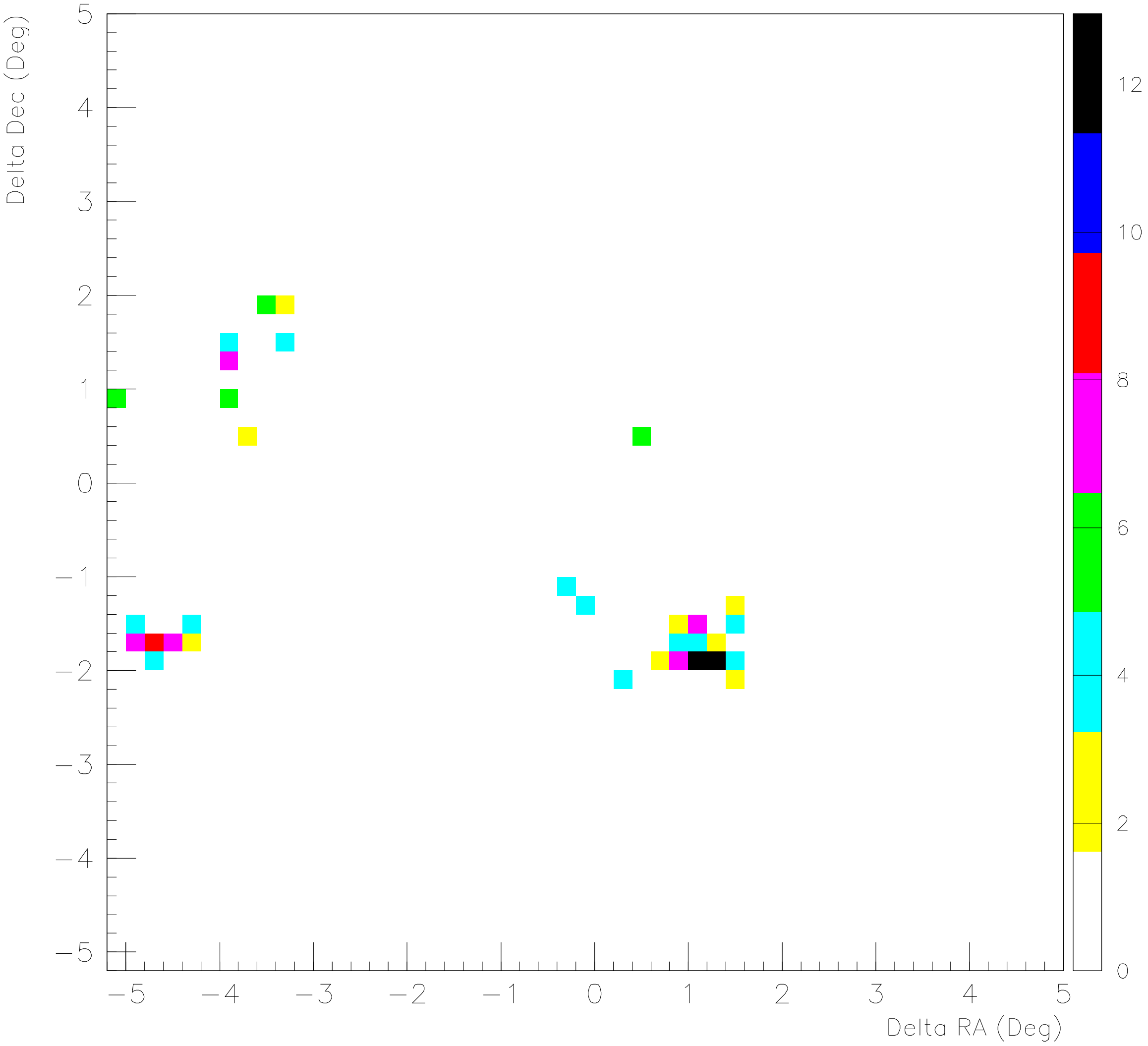

Figure 8: The map of Λ_{max} relative to the position of the Sun, in α and δ from the log-likelihood search for the shadow of the Sun.

The effect of magnetic fields can best be seen by comparing the magnetic fields traversed by a cosmic ray on paths from the Moon to the Earth with the fields experienced on a path from the Sun to the Earth. On the Moon-Earth path, the cosmic ray sees only the Earth's magnetic field; the Moon's field is negligible. To estimate the magnitude of this effect, assume that the fields are uniform in strength and direction. This assumption leads to upper limits on the deflection from the magnetic fields, but it is useful for a comparison between the two systems under discussion. The Earth's magnetic field is ~0.5 G, and extends some $6.4 \text{x} 10^3$ km[5]. The magnetic force upon a particle is given by the Lorentz relation $\boldsymbol{F} = q \cdot \boldsymbol{v} \text{x} \boldsymbol{B}$[13]. Calculating the upper limit leads to evaluation of this force at a cosmic ray direction perpendicular to the magnetic field, so the magnitude of the magnetic force upon a proton becomes $q \cdot v \cdot B$, where q is the charge of the proton, v is the proton's velocity, and B the strength of the magnetic field. Experiencing that force over the length of Earth's magnetic field d imparts an impulse to the proton of $\Delta p = q \cdot v \cdot B \cdot \Delta t = q \cdot d \cdot B$ from Newton's second law[13]. Thus, the proton experiences a maximum momentum change of $\Delta p = 9.6 \text{x} 10^{10}$ eV/c.

For the Sun-Earth trip, the path is dominated by the Sun's magnetic field. Although highly variable, acceptable median values for it are 3 G and $700 \text{x} 10^3$ km[5]. Following the same calculation as above, this imparts a $\Delta p = 6.3 \text{x} 10^{13}$ eV/c to a proton, enough to cause protons up to 30 TeV to lose all directionality. Since the air shower arrays have a far higher energy threshold than MACRO (~100 TeV instead of

~1.2 Tev), the paths of the cosmic rays seen by an air shower array are affected less by the magnetic fields than those seen by MACRO, allowing air showers to observe the shadow of the Sun.

Of course, these numbers are upper limits, but a simple comparison of the Δp's shows the protons passing the Sun to be affected more by the magnetic fields -- by a factor of 650! -- than those passing the Moon. Since the same assumptions were made for each case, the ratio of the real effects should be similar to this ratio of upper limits. This explains why CASA's detection of the Sun's shadow is weak compared to their Moon detection, and why MACRO has been so far unable to observe the Sun's shadow.

Over the integration time of MACRO's dataset, the geometrical angle of incidence between the Earth's magnetic field and cosmic rays from near the position of the Moon or the Sun changes substantially. In the case of the Sun, the magnetic field itself also varies. Thus, the effect of the momentum imparted by the magnetic field is to smear the shadow. The simulated shadow used in this analysis as I_s did not account for any magnetic fields. Since the observed Moon shadow agrees with this simulated shadow, this magnetic smearing must be negligible for Moon to Earth cosmic rays, as hypothesized. However, the lack of a shadow from the sun in the MACRO data indicates a much greater change to the momentum of cosmic rays from the direction of the Sun, washing out the shadow entirely.

4.6 Conclusions

Now MACRO has seen an astronomical object with great significance. No other underground experiment has accomplished this feat. This detection allows a search for sources like Cyg X-3, 3C273, and MRK421 to proceed with the confidence that should these objects somehow be sources of a large enough muon flux to be observable, MACRO will be able to see them. In addition, the assumption that the distribution of double muon space angles well represents MACRO's actual PSF is validated by the high significance of the results obtained when this assumption is used to predict the shadow of the moon.

References

1. Clark, G.W., 1957, ”Arrival Directions of Cosmic-ray Air Showers from the Northern Sky”, *Phys. Rev.* **108**, 450.

2. Alexandreas, D.E. *et al.*, The CYGNUS Collaboration, 1991, “Observations of Shadowing of Ultrahigh-energy Cosmic Rays by the Moon and the Sun”, *Phys. Rev. D* **43**, 1735.

3. Karle, A., Merck, M., Bott-Bodenhausen, M., Kabelschact, A., Holl, I., Lorenz, E., The HEGRA Collaboration, 1991, “Observation of the Shadowing of Cosmic Rays by the Moon and the Sun”, *Proc. 22nd ICRC (Dublin)* **4**, 460.

4. Amenomori, M. *et al.*, The Tibet ASγ Collaboration, 1993, “Cosmic-ray Deficit from the Directions of the Moon and the Sun detected by the Tibet Air Shower Array”, 1993, *Phys. Rev. D* **47**, 2675.

5. Borione, A. *et al.*, The CASA Collaboration, 1993, ”Observation of the Shadows of the Moon and Sun using 100 TeV Cosmic Rays”, *Phys. Rev. D* **49**, 1171.

6. Ahlen, S. *et al.*, The MACRO Collaboration, 1993, “The First Supermodule of the MACRO Detector at Gran Sasso”, *Nucl. Instr. And Meth. Res. A* **324**, 337.

7. Lipari, P., and Stanev, T., 1991, “Propagation of Multi-TeV Muons”, *Phys. Rev. D* **44**, 3543.

8. Standish, E.M., Newhall, X.X., Williams, J.G. and Folkner, W.F., 1995, "JPL Planetary and Lunar Ephemerides, DE403/LE403", *JPL IOM* **314**, 10-127.

9. Duffett-Smith, P., 1988, **Practical Astronomy with your Calculator**, 3rd ed., Cambridge Univ. Press, Cambridge, p.150.

10. Ahlen, S. *et al.*, The MACRO Collaboration, 1992, “Measurement of the Decoherence Function with the MACRO Detector at Gran Sasso”, *Phys. Rev. D* **46**, 4836.

11. Cash, W., 1979, “Parameter Estimation in Astronomy through Application of the Likelihood Ratio”, *Ap. J.* **228**, 939.

12. Pollack, A.M.T., *et al.*, The Caravane Collaboration for the COS-B Satellite, 1985, “COS-B Gamma-Ray Sources and Interstellar Gas in the First Galactic Quadrant”, *Astronomy and Astrophysics* **146**, 352.

13. Weidner, R.T. and Browne, M.E., 1985, **Physics**, Allyn and Bacon, Newton, Mass. pp. 144 and 628.